Journal of Ambient Intelligence and Humanized Computing
https://doi.org/10.1007/s12652-019-01339-6

ORIGINAL RESEARCH

Smartphone-based respiratory rate estimation using photoplethysmographic imaging and discrete wavelet transform

Maha Alafeef[1,2] · **Mohammad Fraiwan**[3]

Received: 9 August 2018 / Accepted: 4 June 2019

Abstract
Respiratory rate is a key vital sign that needs daily monitoring for hospital patients in general and those with respiratory conditions in particular. Moreover, it is a predictor of major heart conditions. Yet, studies have shown that it is widely neglected in hospital care due partially to the discomfort caused by the required equipment. In this paper, we propose a smartphone-based method for accurate measurement of the respiratory rate using the video of the skin surface as recorded by the smartphone built-in camera in the presence of the flash light. From this input, we use frame averaging to extract a photoplethysmographic signal of the red, green, and blue channels. Next, we apply discrete wavelet transform on the best representative photoplethysmographic signal for respiratory signal extraction and estimate the rate. Fifteen subjects participated in the testing and evaluation. The maximum absolute error was 0.67 breaths/min, whereas the root mean square error was 0.366 breaths/min. The average percentage error and average percentage accuracy using our approach were 2.2%, 97.8% respectively. A comparison with other works in the literature reveal a superior performance in terms of accuracy, ease of use, and cost.

Keywords Smartphone · Respiratory rate · Photoplethysmographic · Discrete wavelet transform

1 Introduction

The rapid development in the capabilities of smartphones has led to a plethora of powerful applications. The pervasiveness of the mobile devices into our daily lives presents an opportunity to deploy these devices for healthcare services to mimic the functionality of some medical devices. If the accuracy is acceptable, mobile devices offer several advantages over professional setups in terms of ease of use, the need for health professionals, accessibility, cost, and continuous presence and follow-up.

Respiratory rate (RR) is a major vital sign, which reflects the condition of respiratory system, as well as a marker for the healing progress, and a predictor of major ailments. Some of these include cardiac arrest, sleep disorder, and cardiopulmonary disorders (Cretikos et al. 2008). Also, RR can be used to follow up on drug administration (Schroeder and Smith 2011). In addition, it is a sensitive indicator of acute respiratory dysfunction (Gravelyn and Weg 1980). Although many hospitals use pulse oximetry recording for patient ventilation monitoring, RR can provide information that cannot be obtained using the pulse oximeter only (Cretikos et al. 2008).

The respiratory signal recording is carried out by specialized instruments such as the nasal thermistor, spirometer, pneumography, plethysmography, or capnography. These devices can cause patient discomfort by interfering with natural breathing and are inconvenient for certain applications such as stress testing, ambulatory monitoring, and sleep apnea cases (Bailon et al. 2006). They may also be impractical for continuous RR monitoring because of their low accessibility, poor portability, and operational reliance on trained individuals. Therefore, there is a need to develop a non-invasive, accessible, cost-effective, portable, easy to use, and accurate method for respiratory rate measurement.

✉ Mohammad Fraiwan
mafraiwan@just.edu.jo

Maha Alafeef
alafeef2@illinois.edu

[1] Department of Bioengineering, University of Illinois Urbana-Champaign, Urbana, IL 61801, USA

[2] Department of Biomedical Engineering, Jordan University of Science and Technology, Irbid 22110, Jordan

[3] Department of Computer Engineering, Jordan University of Science and Technology, P. O. Box 3030, Irbid 22110, Jordan

Published online: 10 June 2019

It is possible to estimate RR from a signal called Photo-Plethysmography (PPG). PPG is a waveform obtained from the reflected or transmitted light after illuminating part of the skin surface (e.g., the index or ear lobe) using either infrared or red light. This signal is composed of various frequency components, which relate to respiratory activates, blood pressure, and heart pulsation. Thus, it represents a convenient choice from which the respiratory rate can be extracted. The PPG signal is dominated by two components: one is an alternating signal (AC component), resulting from the pulsatile nature of the blood circulation in the arteries as driven by the heartbeat, and the other is a Quasi-DC component caused by the skin, bone, and tissue, which is not affected much by the respiratory activity (Meredith et al. 2012; Webster 1997).

Smartphones are continuously being equipped with more powerful cameras and flash light. Such capabilities open the avenue for PPG-based solutions that harness the computational power of smart devices and their daily life advantages. In this context, the contributions of this paper are as follows:

1. We collect RR video data of subjects fingertips using mid-range smartphone, along with the Plethysmography signals using dedicated hardware (for validation purposes).
2. We process the collected videos to extract the PPG signals from the appropriate color channels.
3. We use discrete wavelet transform to analyze the collected PPG signals and estimate the RR.
4. Using our system, the patient can measure his/her RR by just inserting his/her fingertip over the mobile phone camera. This paper demonstrates the ability and the feasibility of using smartphones for healthcare application without the need for extra hardware.

The rest of this paper is organized as follows. In Sect. 2 we discuss and analyze the related work done in the literature. Section 3 goes into the details of data collection, PPG signal extraction, and the respiratory rate estimation. We present the results of the RR estimation in Sect. 4. We conclude in Sect. 5.

2 Background and related work

Mobile healthcare (mhealth) is a trending branch of eHealth, which is capitalizing on the ubiquity and spread of smartphones and wearable sensors. The applications of mhealth include the collection of clinical medical data, remote diagnosis, monitoring, collaboration, and awareness. The research into these areas has increased in sophistication and breadth. A comprehensive study of remote patient monitoring is discussed by Malasinghe et al. (2019). In this context, Chen and Chiu (2018) present a review of the literature in connection to life quality in mobile environments, and a procedure/model for the application of smart technologies. Moreover, smart mobile healthcare has ventured into Magnetic Resonance Imaging (MRI) (Nie et al. 2018), cancer research (Jamil et al. 2019), and physiological data collection (Tambe and Gajre 2018).

The PPG non-invasive nature makes it a popular choice for ubiquitous computing medical applications. More specifically, it can provide a platform for continuous monitoring of the respiratory and cardiovascular systems (Moraes et al. 2018). For example, the PPG signal has been employed to monitor the heart rate and its variability (Alafeef 2017; Hassan et al. 2017; Sanyal and Nundy 2018). In addition, advancement in sensors and signal processing techniques (Kao et al. 2019; Pirhonen et al. 2018; Tabei et al. 2018) improves the reliability, accuracy, and robustness of the PPG-based applications.

Charlton et al. (2018) present a recent literature review of the RR estimation from PPG signals. Several algorithms and techniques for RR extraction have been developed in the past few years (Karlen et al. 2015; Leonard et al. 2006; Li 2016; Mitali and Prabhu 2015; PS and Jatti 2015). Li (2016) proposed an Android mobile app that employs the smartphone sensors (i.e., accelerometer and gyroscope) for respiratory rate estimation. They used signal filtration and further processing to estimate the RR with an error of ± 2 breaths/minute, which is high. In their approach, the respiratory signals need to be collected from the abdomen and chest areas, which may be inconvenient. Mitali and Prabhu (2015) used an Ensemble Empirical Mode Decomposition (EEMD) algorithm for RR extraction from the PPG signal obtained using an optical sensor. They add white noise to the signal in order to decompose it into Intrinsic Mode Functions (IMFs), and use the ensemble mean of the IMF to achieve an average accuracy and maximum absolute error of 97%, and 1.01 breaths/min, respectively. Although they were able to estimate the respiratory rate with high accuracy, the use of an external device such as pulse oximeter for PPG signal extraction reduces the system portability and cost. Moreover, the range at which the algorithm was tested is very narrow (14–18 breaths/min), which brings into question the applicability over higher RRs. Furthermore, the EEMD algorithm requires high computational power and processing time because of the required iterations for IMFs extraction, which affects the practical and real-time deployment of such system.

Leonard et al. (2006) introduced an automated method for respiratory rate measurement in children using PPG obtained using a pulse oximeter device. They used wavelet transform to extract the RR. For performance evaluation, they compared the estimated values with values recorded by an observer activating a push-button switch in synch with

breathing. Although the error rate was 1 breath/min, the use of a pulse oximeter for PPG signal recording reduces the system portability and cost. In another study, Karlen et al. (2015) recorded videos, using a smartphone, from 19 subjects and applied Smart Fusion and Empirical Mode Decomposition (EMD) on the PPG signal. They used Capnometry for the reference rates. They reported a high value of the root mean square error (RMSE) of 6 breaths/min, which is unsatisfactory. The RMSE based on the pulse oximeter signal was 2.3 breaths/min. The error is lower than the smartphone-based estimation, but it is still high.

PS and Jatti (2015) designed a circuit for PPG signal recording and filtration. They discussed the implementation of the wavelet decomposition technique for RR estimation, and the results are reported to the physician's mobile phone. The maximum absolute error was found to be 4 breaths/min, which is very high and requires external circuitry. Additional circuitry is also required by the work of Lin et al. (2017), who proposed to implement a wavelet-based algorithm into a micro-controller (MCU) that can be embedded in a pulse oximeter. They report a $\pm$ 1 breath/min accuracy, but over short 10-s segments, which is high considering the typical number of breaths in 10 s (i.e., less than 3). In addition, they select five long-term recordings (i.e., > 10 min), which is not enough to get a good indication of accuracy. Similarly, their work in (Lin et al. 2013) reports the results from one subject, which is unacceptable.

3 Materials and methods

Figure 1 shows the steps involved in obtaining the video recording and the processing steps. In the following subsections, we go through the steps in details.

3.1 Volunteers

We examined the system performance using 15 subjects. The age of the volunteers ranged from 19 to 52 years and the estimated respiratory rate was in the range of 7.5–28.6 breaths/min, which more than covers the normal range of respiration (Barrett et al. 2019). None of them had any chronic disease. We explained the test procedure to each volunteer, and then every subject signed a consent form before data collection. The institutional review board (IRB) of Jordan University of Science and Technology granted all the necessary ethical permissions. The study was conducted in accordance with the declaration of Helsinki.

3.2 Data collection

We recorded four types of data concurrently, as follows:

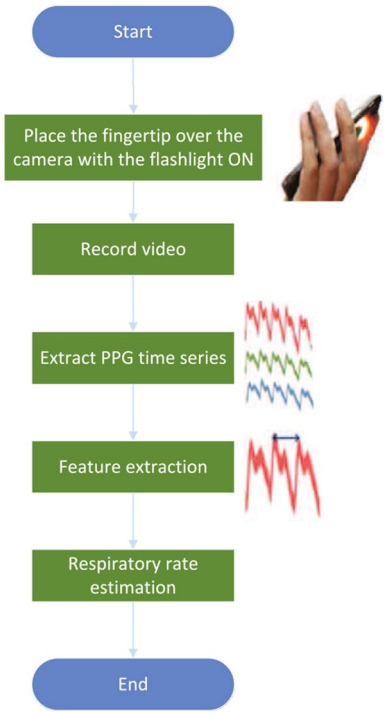

Fig. 1 The system flowchart

1. Using the built-in camera of a Samsung Galaxy S6 smartphone, we recorded a video from each subject's index fingertip with 30.30 frames per s, RGB24, and 1280×720 resolution, with the flashlight on. The finger must cover both the flashlight and the camera in order to obtain useful data. Moreover, subjects were instructed to make themselves comfortable. The breathing rate was measured during rest with a flow sensor, and the subjects were instructed to inhale and exhale at the measured rate with the help of a metronome-like repeating tone.
2. The Plethysmography signal was recorded using a specialized sensor attached to the IWX/214 data acquisition unit (iWorkx 2018a) and displayed using LabScribe (iWorkx 2018b). The purpose of this simultaneous measurement is to verify that the PPG signal extracted from the smartphone is able to detect the actual blood flow waveform without any missed peaks. The Strain gage sensor is sensitive to the changes caused by the cardiac action and is able to detect a similar signal to the PPG. It represents a standardized technique for Plethysmography waveform recording (Almond et al. 1988; SINGH 2014).
3. The respiratory signal using a flow sensor.
4. The RR using an observer with a stopwatch.

The later two recordings complement each other to make sure that we got an accurate RR count and rhythm, and they were used for performance comparison. The system

computes the respiratory rate based on the extracted respiratory signal from the smartphone video as stated earlier.

3.3 PPG signal extraction

The following steps are involved in the PPG signal extraction:

1. Decompose the video into individual frames, where each frame represents an RGB image.
2. Extract red, blue, and green averaged intensities from the individual video frames by averaging the corresponding pixel intensities for all the pixels in the frame. Thus, we get three values associated with each frame (i.e., the red, green, and blue intensities). The averaging is necessary to eliminate the effect of spatial variation.
3. Record the time associated with each frame, see Eq. 1. Figure 2 shows the PPG time series as intensity values change with time. Although three channels were obtained from the video processing, not all of them can give a clear PPG waveform. Thus, we used the most appropriate one, which is the red channel, without the need for any additional processing or filtration. The PPG signals from both the green and blue channels are unclear and require complex additional processing to obtain useful information.
4. Each frame gives a single value, which represents the PPG signal amplitude of each channel at the time of capturing the frame. This is true for all frames. When the average intensity of each channel is computed for all video frames, the PPG waveform is produced by plotting the intensity of the desired channel for all frames as a function of time.

$$Time = \frac{frame\ number\ of\ each\ intensity\ value}{frame\ rate} \tag{1}$$

3.4 Multilevel wavelet decomposition

Aside from the Quasi-DC component mentioned earlier, the PPG signal is dominated by two frequency components, the first is concentrated around 1 Hz and represents the pulsatile component in connection to the blood flow in the vessels, whereas the second one is in the range of 0.2–0.33 Hz and relates to the periodic respiratory signal of healthy subjects. Figure 3 shows the scalogram of a sample of the collected data. This plot provides information about the frequency content of the signal at each time point. It is clear that the heartbeat signal is in the higher frequency range and the RR is in the lower portion of the plot (Murthy et al. 2001). We break down this scalogram and select the frequency region of interest.

Time–frequency data can be extracted using wavelet transform, which is an efficient signal processing technique for the analysis of non-stationary transient signals. It provides a representation of a time–series signal in terms of simple component blocks, known as wavelets. A single generating function, called the mother wavelet, is used to derive these blocks. The mother wavelet generates a

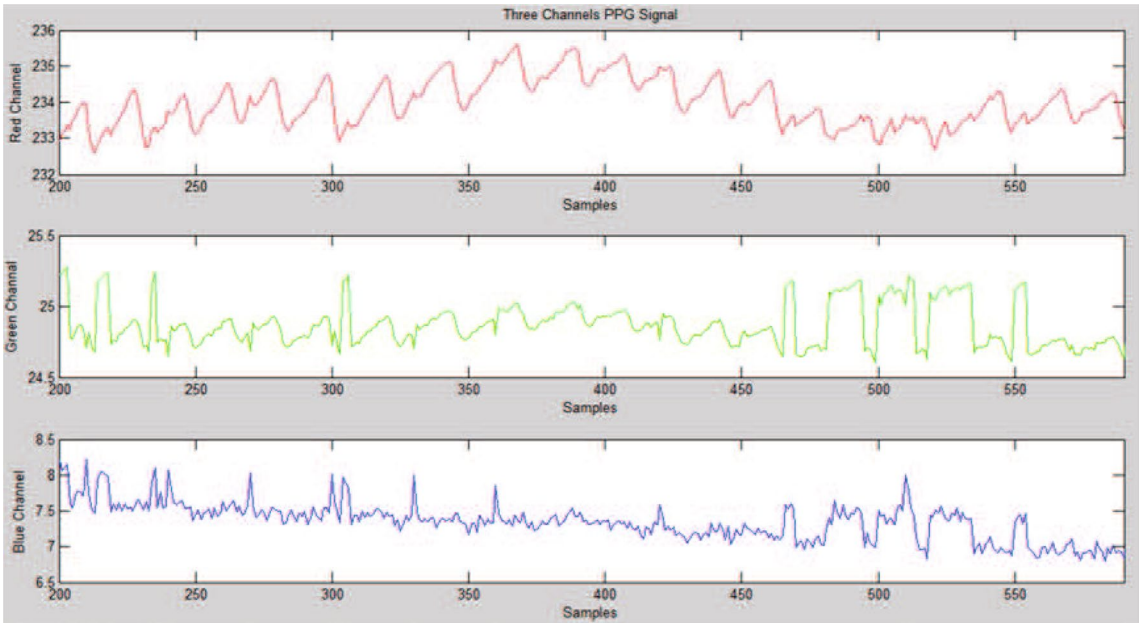

Fig. 2 The PPG signal extracted from the red (top), green, and blue (bottom) components

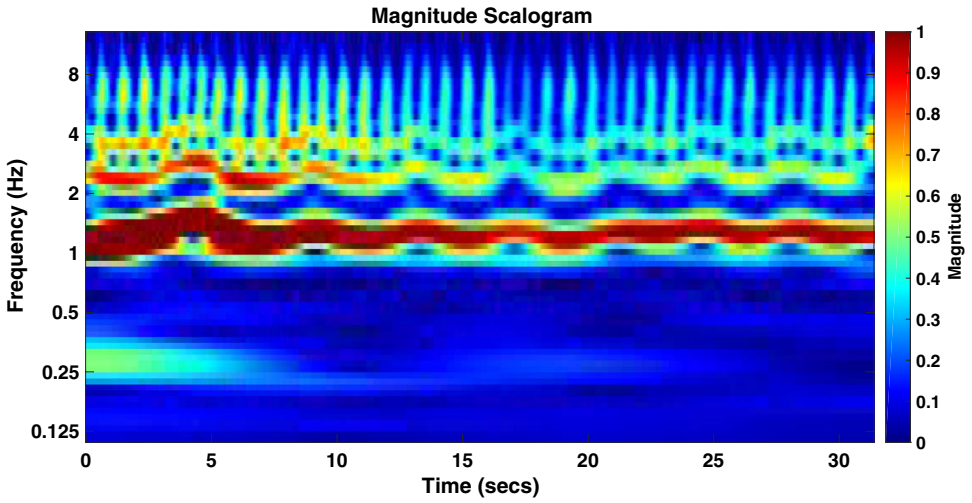

Fig. 3 The scalogram of a random subject. The heartbeat signal is in the higher frequency range, while the RR is close to 0.25–0.4 Hz

family of functions by translating/shifting the mother function along the time axis and applying the dilation operations (i.e., compressing or stretching operations). Wavelet decomposition has been used for feature extraction because it analyzes the signal both in time and frequency (Daubechies 1990; Soltani 2002; Ubeyli and Guler 2005; Unser and Aldroubi 1996). The continuous wavelet transform (CWT) is computed based on Eq. 2:

$$CWT = \int_{-\infty}^{+\infty} x(t)\psi_{a,b}(t)dt \tag{2}$$

$\psi(t)$ is known as the mother wavelet and $\psi_{a,b}(t)$ is the dilation and transformation of $\psi(t)$, see Eq. 3. b is a time shifting parameter that captures the time domain characteristics of the signal $x(t)$. a is a scaling parameter, which provides the mother wavelet function $\psi(t)$ dilation and compression characteristics.

$$\psi_{a,b}(t) = \frac{1}{\sqrt{|a|}}\psi\left(\frac{t-b}{a}\right) \tag{3}$$

Discrete wavelet transform (DWT) is the discretized version of the CWT that captures the important features of the original signal. In other words, it compresses the signal and reduces the computational complexity of the highly redundant CWT, while maintaining a high-quality representation. In DWT, the signal is decomposed into approximation (low pass filter) coefficients and detail coefficients (high pass filter), followed by downsampling. The resulting approximation coefficient is further split into two parts using the same procedure. For example, if the wavelet transform is used to decompose the signal at level k, the wavelet decomposition will have the following structure: $[A_k D_k D_{k-1} D_{k-2} \ldots D_2 D_1]$. Figure 4 illustrates the structure of the wavelet decomposition of the signal S at three levels.

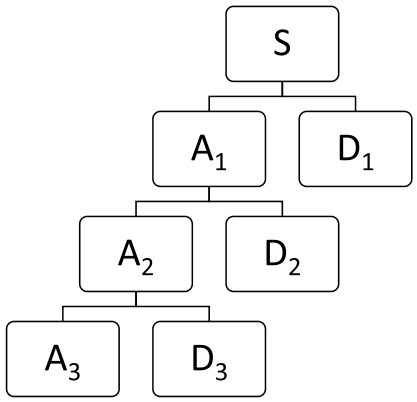

Fig. 4 Three-level discrete wavelets transform decomposition

The proper selection of the number of decomposition levels and the mother wavelet is critical in the signal analysis by DWT. The decomposition level depends on the RR frequency of interest and the sampling frequency. For example, level 7 will disclose frequency information about a respiratory rate as low as 7 breaths/min for a sampling frequency of 30 fps. In the case of other capturing devices with different sampling frequency, Eq. 4 relates the decomposition level with the sampling frequency, and how the level can be adjusted to reveal the minimum RR frequency of interest (Giurgiutiu 2014).

$$Level = \left\lceil \log_2 \frac{Sampling\ freq.}{min.\ RR\ freq.} - 1 \right\rceil \tag{4}$$

In our case, we chose the number of decomposition levels to be nine (i.e., detail: $D_1 \ldots D_9$ and one approximation: A_9). This level will disclose frequency information about a respiratory rate as low as 4 breaths/min. We experimented with different types of the mother wavelet and settled on

using the Daubechies (1990) wavelet of order 2 (i.e., db2) because of its smoothing feature. The calculated wavelet coefficients based on db2 were found to be suitable to detect RR changes, which are embedded within the PPG signal. Figure 5 shows the results of the decomposition of the PPG signal (red channel) using DWT.

We extracted the respiratory signal by selecting suitable detail coefficient results from the original PPG signal decomposition and used the selected detail coefficient for RR calculation. We chose the detail coefficient based on the frequency response that matched the frequency of the respiratory signal. In this work, the detail coefficient d_7 as shown in Fig. 5 represents the respiratory activity of the subject with the PPG signal denoted by s. Figure 6 illustrates the red channel PPG signal extracted from selected video and its corresponding extracted respiratory signal using DWT. The discrete wavelet coefficients were calculated using MATLAB 2017a (MathWorks 2018).

3.5 Respiratory rate estimation

In order to estimate the RR, we located the peaks of the respiratory signal by applying a standard peak detection algorithm on the DWT-extracted signal. After that, we calculated the time between each two consecutive peaks, which represents the time of one respiration. The time is taken to complete one respiratory cycle is calculated from the number of frames between two consecutive maxima divided by the frame rate as in Eq. 5. After that, we used the average cycle time over the whole signal to compute the respiratory rate estimation as shown in Eq. 6.

As for the error calculation, a multitude of measures may be used and they can be considered for a given subject (i.e., segment by segment or cycle by cycle) or across subjects (i.e., for all of the recording period of each subject), as follows, where i in Eqs. 8 and 10 can be cycles, segments, or subjects:

- The absolute error and mean absolute percentage error (MAPE) in Eqs. 7 and 8 respectively. The maximum absolute error gives an indication of the largest error in the rates, but without consideration to the differences in magnitude of the actual rates (e.g., an error of 4 out of 30 should better than 3 out of 20). On the other hand, MAPE is the normalized mean of the relative error, which accounts for different magnitude scales of the actual rates and is easier to interpret than RMSE. In this case, the accuracy is 100% - MAPE (i.e., the mean value of Eq. 9).
- The root mean square error (RMSE), see Eq. 10. RMS will penalize large error values due to squaring the errors before taking the square root, which makes it sensitive to outliers.

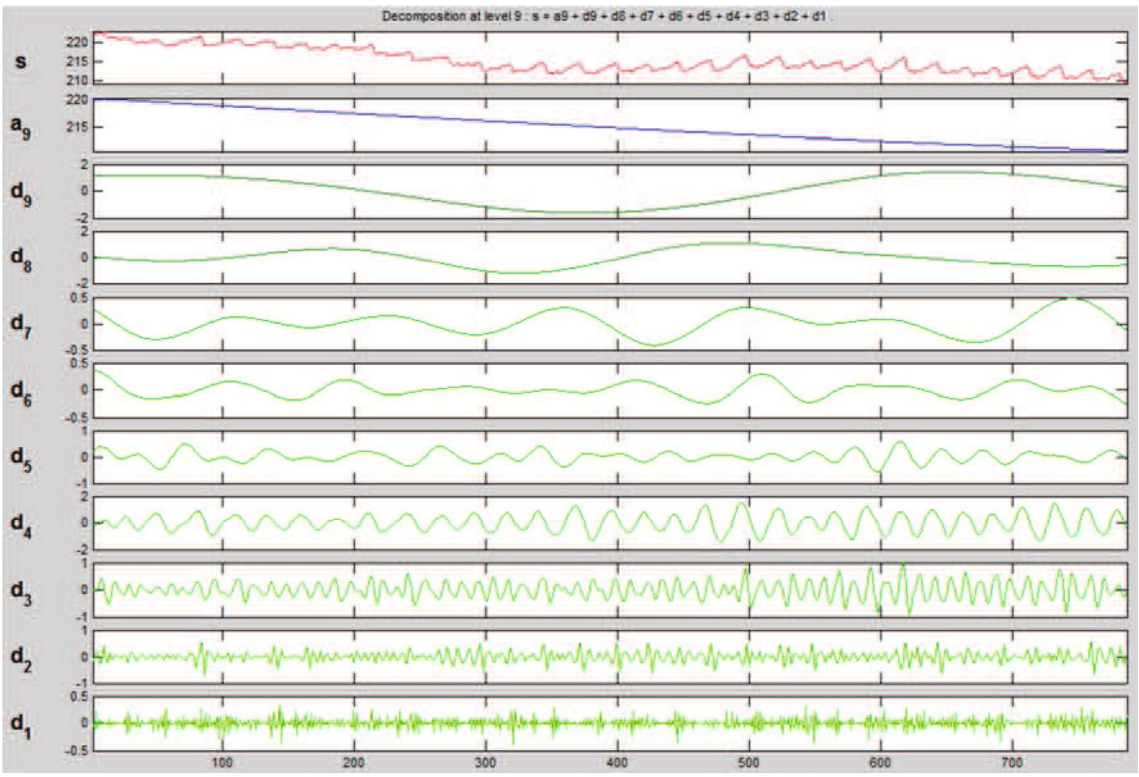

Fig. 5 Nine-level wavelet decomposition of a PPG signal extracted from the video stream

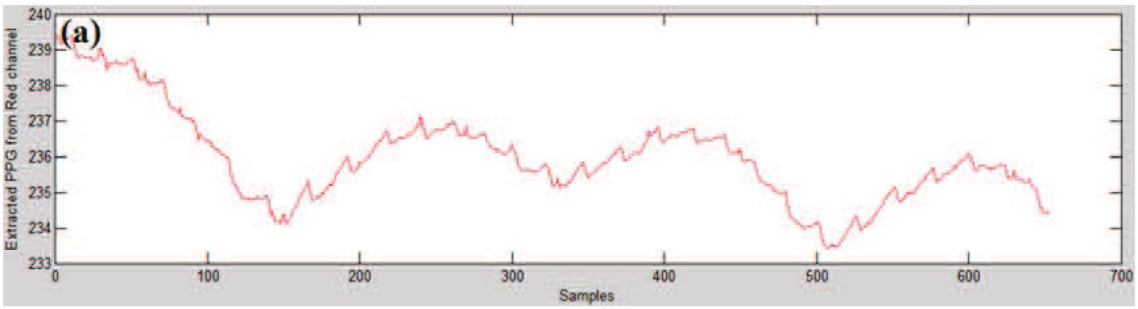

The PPG signal extracted from the red component.

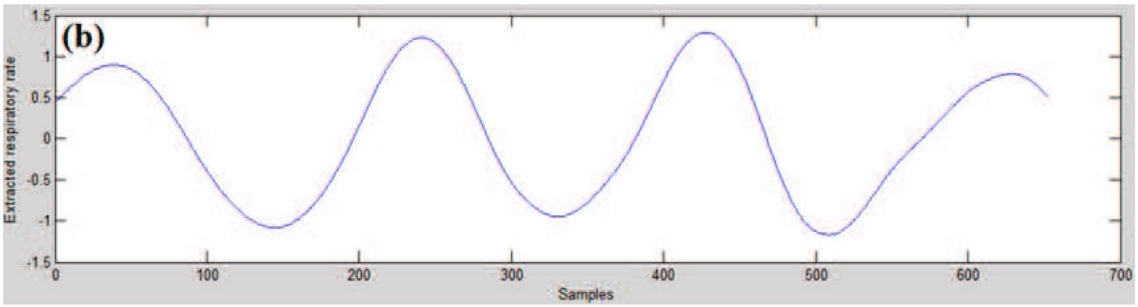

The respiratory signal.

Fig. 6 A comparison of the PPG signal, as extracted from the red component, against the estimated respiratory signal

Moreover, RMSE requires further normalization for it to be scale-independent.

- The Bland–Altman plot, which is a very useful technique for the evaluation of estimation agreement with the actual rate. If the 95% of the data points are within the mean$\pm 1.96 \times SD$ range, then the methods of estimation and measurement can be used interchangeably (Bland and Altman 1986).

$$Time\ of\ one\ cycle = \frac{Number\ of\ frames}{Frame\ rate\ (fr/sec)} sec/one\_cycle \tag{5}$$

$$Respiratory\ rate = \frac{60}{Avg.\ cycle\ time} breaths/minute \tag{6}$$

$$Absolute\ error = |Actual\_RR - Estimated\_RR| \tag{7}$$

$$MAPE = \frac{1}{n} \sum_i \frac{|Actual\_RR_i - Estimated\_RR_i|}{Actual\_RR_i} \times 100\% \tag{8}$$

$$Accuracy = \left(1 - \frac{Absolute\ error}{Actual\_RR}\right) \times 100\% \tag{9}$$

$$RMSE = \sqrt{\frac{1}{n} \sum_i (Actual\_RR - Estimated\_RR)^2} \tag{10}$$

4 Results and discussion

We evaluated the proposed approach on the collected data of the 15 subjects by comparing the extracted RR with the measured value. Table 1 shows the RR values of the actual rate and the corresponding PPG-based estimation in terms of the absolute error. The actual rate data was for paced breathing and showed little variance throughout the recordings. Across different subject, the average percentage error and the average percentage accuracy were 2.2%, 97.8% respectively, which surpasses the comparable literature (Karlen et al. 2015; Leonard et al. 2006; Li 2016; Mitali and Prabhu 2015; PS and Jatti 2015). The same applies to the maximum error, which was 0.67 breaths/min. Moreover, most of the absolute error values are lying within the range [0.1–0.5] breaths/min, with a mean of 0.33 and a median of 0.35. In addition, the correlation between the RR and the absolute error was 0.31, which indicates a weak relationship. The absolute error holds a similar correlation to the RR with a value of 0.28.

Figure 7 shows the extracted RR using the smartphone versus the actual RR. Each point in the plot represents the estimated respiratory rate of one subject with the corresponding actual respiratory rate. The closer the point to the diagonal line, the lower the error. As we can see, most of the data points lie closer to the diagonal line and reveal very small estimation error. Figure 8 shows the percentage error of RR estimation of each one of the 15 subjects. The

Table 1 Comparison between the actual RR and the corresponding PPG-based estimated respiratory rate in terms of the absolute error and accuracy. [a] mean ± standard deviation

Sub. No.	Actual RR (% ± *SD*)[a]	RR using PPG (% ± *SD*)[a]	Abs Error (% ± *SD*)[a]	Accuracy (% ± *SD*)[a]
1	13.71 ± 0.206	13.04 ± 0.19	0.67 ± 0.004	95.11% ± 0.25%
2	14.29 ± 0.213	14.39 ± 0.2	0.1 ± 0.011	99.28% ± 0.16%
3	11.54 ± 0.203	11.39 ± 0.17	0.15 ± 0.01	98.73% ± 0.25%
4	8.57 ± 0.196	8.78 ± 0.173	0.21 ± 0.017	97.56% ± 0.41%
5	12 ± 0.211	12.5 ± 0.18	0.5 ± 0.012	95.83% ± 0.22%
6	11.76 ± 0.219	11.39 ± 0.18	0.37 ± 0.013	96.83% ± 0.24%
7	19.35 ± 0.256	18.95 ± 0.19	0.4 ± 0.02	97.88% ± 0.15%
8	23.08 ± 0.293	22.78 ± 0.19	0.3 ± 0.022	98.73% ± 0.23%
9	7.5 ± 0.111	7.38 ± 0.09	0.12 ± 0.004	98.36% ± 0.22%
10	17.65 ± 0.33	17.82 ± 0.21	0.17 ± 0.018	99.02% ± 0.25%
11	15.79 ± 0.309	16.07 ± 0.235	0.28 ± 0.019	98.21% ± 0.25%
12	19.35 ± 0.347	18.95 ± 0.27	0.4 ± 0.021	97.88% ± 0.21%
13	28.57 ± 0.665	28.13 ± 0.448	0.44 ± 0.038	98.44% ± 0.29%
14	17.14 ± 0.226	16.67 ± 0.213	0.47 ± 0.018	97.22% ± 0.16%
15	17.65 ± 0.415	18 ± 0.305	0.35 ± 0.026	98.02% ± 0.2%

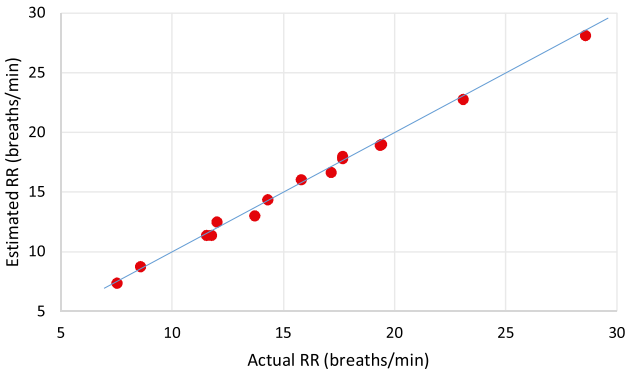

Fig. 7 Respiratory rate estimation versus the actual rate. Each point represents the estimated RR vs the actual RR for one subject. The total is 15 subjects

percentage error of those subjects found to lie within the range of [0.72–4.89%] with a mean of 2.2% and a median of 2%.

We used the Bland–Altman plot in Fig. 9 to evaluate the agreement between the estimated RR and the actual rate. The graph shows that there is a slight mean system bias with a value of 0.115 breaths/min. The difference values are tightly arranged around the mean bias with all points located within the limit of agreement (i.e., mean $\pm 1.96 \times SD$). Therefore, our method can be used interchangeably with the existing respiratory rate measuring techniques and provide reliable results. Furthermore, the plot shows that there is no rate-dependent error. Figure 10a shows an actual respiratory signal recorded using the digital spirometer, whereas Fig. 10b illustrates the respiratory signal extracted from the

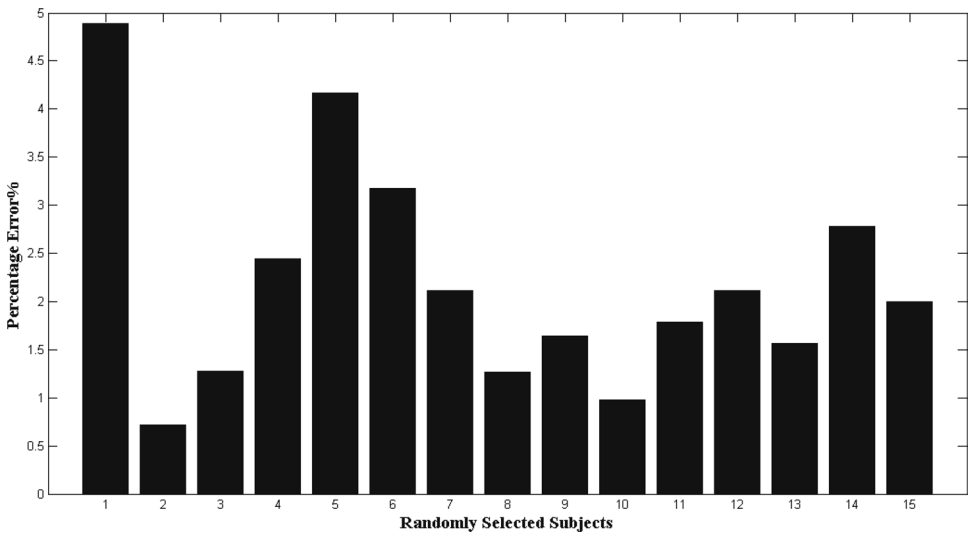

Fig. 8 Error percentage of the respiratory rate estimation from the 15 subjects. The error is measured over all of the recording period

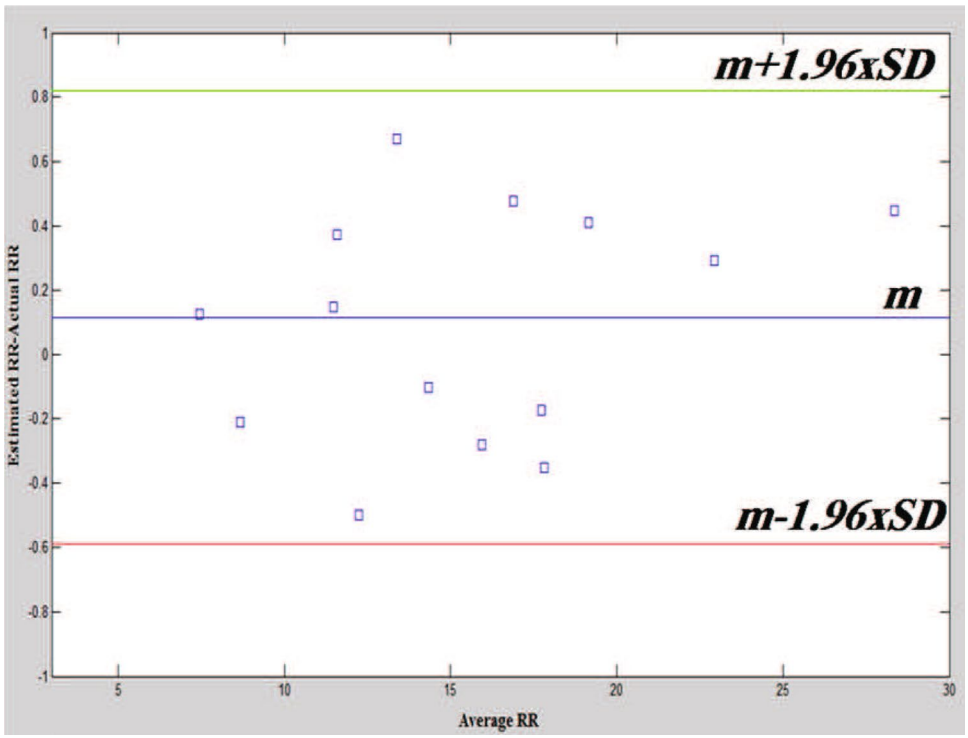

Fig. 9 Bland–Altman plot of the results in Table 1. The horizontal lines represent the mean bias level and the 1.96 standard deviation from the bias mean

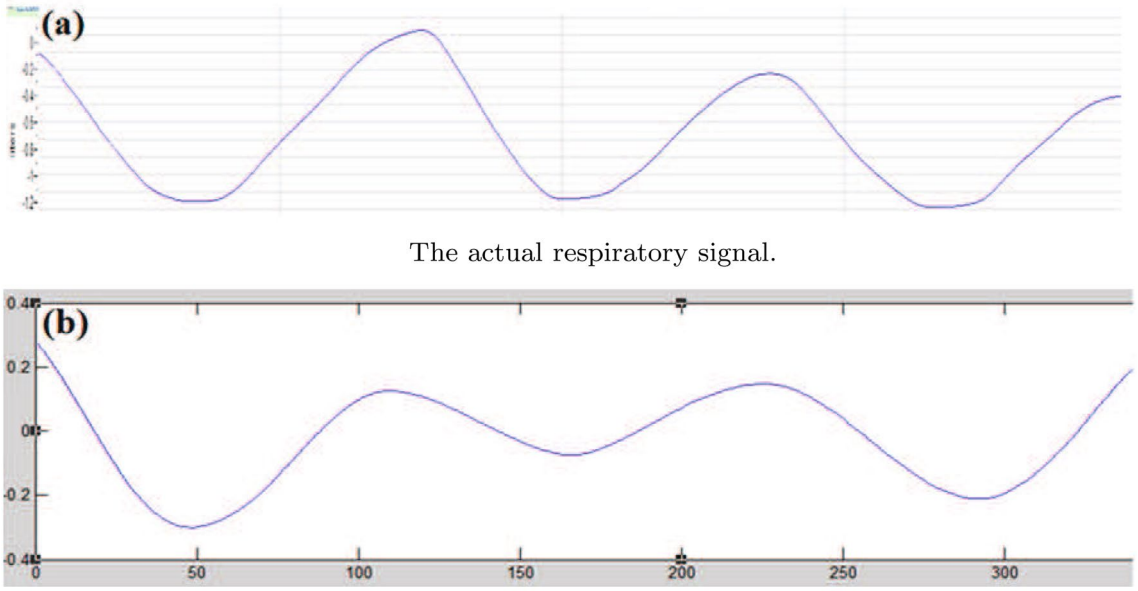

Fig. 10 A comparison of the actual respiratory signal recorded from a randomly selected subject and the extracted respiratory signal using DWT

same subject using our system (smartphone PPG and DWT). It is clear that the two signals are almost identical, which serves as an evidence about the accuracy and efficacy of the developed system.

Figure 11 shows a comparison between the maximum absolute errors obtained using our system against the reported results in the literature (Karlen et al. 2015; Leonard et al. 2006; Li 2016; Mitali and Prabhu 2015; PS and Jatti 2015). It is clear that the maximum absolute error of our approach (i.e., 0.67 breaths/min) is minimal relative to the error values of the other methods. Although the error values reported in (Leonard et al. 2006; Mitali and Prabhu

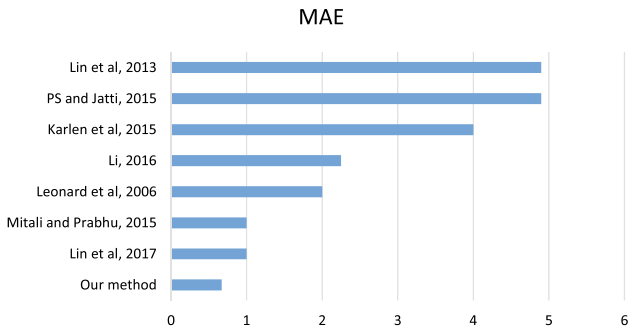

Fig. 11 A comparison of the Maximum Absolute Error in the literature

2015) are close (i.e., 1.01 and 1 breaths/min, respectively), our approach offers portability, cost-efficiency, and ease of use. For example, in (Mitali and Prabhu 2015) the use of a pulse oximeter for PPG signal extraction reduces the system portability and increases the system price. Furthermore, the range they used to test their algorithm was very narrow (14–18 breaths/min) and the EEMD algorithm is computationally intensive and power consuming because of the iterative nature of the IMFs extraction.

The features and computational power of smartphones are increasing rapidly, which has the potential to enable a great number of medical applications. In the context of RR estimation, it is safe to say that current video frame rates (i.e., 30 fps) of commercial smartphones are highly adequate for RR estimation from PPG signals. Moreover, high-end smartphones do support up to 120 fps, which although high but is not required for this type of application. According to Ganon's Review of Medical Physiology (Barrett et al. 2019), the normal range of the RR is between 12–18 breaths/min, which corresponds to a frequency range of 0.2–0.3 Hz. In some cases, and age groups (e.g., elderly over 80 or newborn/infants), it can reach 30 breaths/min (0.5 Hz). The range of the RR in our study is 7.5–28, which covers this wide range of cases and can be detected with high accuracy as demonstrated by the results. In the extreme case, a pathological and dangerous 1Hz RR (i.e., 60 breaths/min) is easily detectable with 30 fps (i.e., 30 Hz).

5 Conclusion and future work

The pervasiveness and ubiquity of mobile smartphone technology coupled with the strong computational power of these devices, presents an excellent opportunity to develop applications that bring healthcare to the patient. In this paper, we presented a complete system for respiratory rate estimation with superior accuracy. The smartphone building camera, which is improving in capabilities with every new model, provides the input to the system as a video of the subject's fingertip. This video stream is the source of the PPG signal (i.e., respiratory signal extraction) and the RR estimation. There is no need for any extra hardware. In comparison to the literature, our stand-alone solution is highly accurate with a maximum absolute error of 0.67 and a 97.7% accuracy, portable as it relies on the smartphone only, cheap, computationally feasible as it does not require highly complicated mathematical procedures, and easy to use as the subject can measure her/his respiratory rate without the need to be in a hospital or a clinic.

Future work will focus on developing a mobile application encompassing our ideas along with the Matlab functions hardcoded with a suitable graphical frontend. Moreover, this research can be expanded further to include different data analysis methods and experimental setup to account for different temperature conditions (e.g., very cold or very warm), skin color, skin conditions (e.g., hardened rough skin vs smooth), age groups, paced breathing, and fast breathing (e.g., during or after workout). In addition, performance evaluation in terms of smartphone battery life/power consumption and speed of processing can also be studied.

Funding This research was supported by Jordan University of Science and Technology, Deanship of Research award number 20180356.

References

Alafeef M (2017) Smartphone-based photoplethysmographic imaging for heart rate monitoring. J Med Eng Technol 41(5):1–9. https://doi.org/10.1080/03091902.2017.1299233

Almond NE, Jones DP, Cooke ED (1988) Noninvasive measurement of the human peripheral circulation: relationship between laser doppler flowmeter and photoplethysmograph signals from the finger. Angiology 39(9):819–29

Bailon R, Sornmo L, Laguna P (2006) A robust method for ecg-based estimation of the respiratory frequency during stress testing. IEEE Trans Biomed Eng 53(7):1273–85. https://doi.org/10.1109/tbme.2006.871888

Barrett KE, Barman SM, Scott Boitano HLB (2019) Ganong's review of medical physiology, 26th edn. McGraw-Hill, New York

Bland JM, Altman D (1986) Statistical methods for assessing agreement between two methods of clinical measurement. Lancet 327(8476):307–310. https://doi.org/10.1016/S0140-6736(86)90837-8, http://www.sciencedirect.com/science/article/pii/S0140673686908378, originally published as Volume 1, Issue 8476

Charlton PH, Birrenkott DA, Bonnici T, Pimentel MAF, Johnson AEW, Alastruey J, Tarassenko L, Watkinson PJ, Beale R, Clifton DA (2018) Breathing rate estimation from the electrocardiogram and photoplethysmogram: a review. IEEE Rev Biomed Eng 11:2–20. https://doi.org/10.1109/RBME.2017.2763681

Chen T, Chiu MC (2018) Smart technologies for assisting the life quality of persons in a mobile environment: a review. J Ambient Intell Humaniz Comput 9(2):319–327. https://doi.org/10.1007/s12652-016-0396-x

Cretikos MA, Bellomo R, Hillman K, Chen J, Finfer S, Flabouris A (2008) Respiratory rate: the neglected vital sign. Med J Aust 188(11):657–9

Daubechies I (1990) The wavelet transform, time-frequency localization and signal analysis. IEEE Trans Inf Theory 36(5):961–1005. https://doi.org/10.1109/18.57199

Giurgiutiu V (2014) Chapter 14-signal processing and pattern recognition for structural health monitoring with pwas transducers. In: Giurgiutiu V (ed) Structural Health Monitoring with Piezoelectric Wafer Active Sensors (2nd Edn), second edition edn, Academic Press, Oxford, pp 807 – 862, https://doi.org/10.1016/B978-0-12-418691-0.00014-9, http://www.sciencedirect.com/science/article/pii/B9780124186910000149

Gravelyn TR, Weg JG (1980) Respiratory rate as an indicator of acute respiratory dysfunction. JAMA 244(10):1123–5

Hassan M, Malik A, Fofi D, Saad N, Karasfi B, Ali Y, Meriaudeau F (2017) Heart rate estimation using facial video: a review. Biomed Signal Process Control 38:346–360. https://doi.org/10.1016/j.bspc.2017.07.004, http://www.sciencedirect.com/science/article/pii/S1746809417301362

iWorkx (2018a) The iworx 214 and labscribe v2.0 tutorial. http://www.iworx.com/wp-content/uploads/2013/02/Tutorial-LS2.pdf. Accessed 26 May 2018

iWorkx (2018b) Labscribe. https://www.iworx.com/research/software/labscribe/. Accessed 26 May 2018

Jamil U, Sajid A, Hussain M, Aldabbas O, Alam A, Shafiq MU (2019) Melanoma segmentation using bio-medical image analysis for smarter mobile healthcare. J Ambient Intell Humaniz Comput. https://doi.org/10.1007/s12652-019-01218-0

Kao Y, Chao PC, Wey C (2019) Design and validation of a new ppg module to acquire high-quality physiological signals for high-accuracy biomedical sensing. IEEE J Sel Top Quantum Electron 25(1):1–10. https://doi.org/10.1109/JSTQE.2018.2871604

Karlen W, Garde A, Myers D, Scheffer C, Ansermino JM, Dumont GA (2015) Estimation of respiratory rate from photoplethysmographic imaging videos compared to pulse oximetry. IEEE J Biomed Health Inform 19(4):1331–8. https://doi.org/10.1109/jbhi.2015.2429746

Leonard PA, Clifton D, Addison PS, Watson JN, Beattie T (2006) An automated algorithm for determining respiratory rate by photoplethysmogram in children. Acta Paediatr 95(9):1124–8. https://doi.org/10.1080/08035250600612280

Li X (2016) Using mobile phone sensors to detect rapid respiratory rate in the diagnosis of pneumonia. Int J Eng Technol 8(4):293–296. https://doi.org/10.7763/ijet.2016.v8.900

Lin YD, Ho HY, Tsai CC, Wang SF, Lin KP, Chang HH (2013) Simultaneous heartbeat and respiration monitoring using ppg and riiv on a smartphone device. Biomed Eng Appl Basis Commun 25: https://doi.org/10.4015/S1016237213500415, https://www.worldscientific.com/doi/abs/10.4015/S1016237213500415

Lin YD, Chien YH, Chen YS (2017) Wavelet-based embedded algorithm for respiratory rate estimation from ppg signal. Biomed Signal Process Control 36:138–145. https://doi.org/10.1016/j.bspc.2017.03.009, http://www.sciencedirect.com/science/article/pii/S1746809417300599

Malasinghe LP, Ramzan N, Dahal K (2019) Remote patient monitoring: a comprehensive study. J Ambient Intell Humaniz Comput 10(1):57–76. https://doi.org/10.1007/s12652-017-0598-x

MathWorks (2018) Matlab. https://www.mathworks.com/products/matlab.html. Accessed 26 May 2018

Meredith DJ, Clifton D, Charlton P, Brooks J, Pugh CW, Tarassenko L (2012) Photoplethysmographic derivation of respiratory rate: a review of relevant physiology. J Med Eng Technol 36(1):1–7. https://doi.org/10.3109/03091902.2011.638965, http://www.ncbi.nlm.nih.gov/pubmed/22185462

Mitali R, Prabhu S (2015) A novel algorithm to obtain respiratory rate from the ppg signal. Int J Comput Appl 126(15):9–12. https://doi.org/10.5120/ijca2015906263

Moraes JL, Rocha MX, Vasconcelos GG, Vasconcelos Filho JE, De Albuquerque VHC, Alexandria AR (2018) Advances in photopletysmography signal analysis for biomedical applications. Sensors 18(6), https://doi.org/10.3390/s18061894, http://www.mdpi.com/1424-8220/18/6/1894

Murthy VS, Ramamoorthy S, Srinivasan N, Rajagopal S, Rao MM (2001) Analysis of photoplethysmographic signals of cardiovascular patients. In: Conference Proceedings of the 23rd Annual International Conference of the IEEE Engineering in Medicine and Biology Society, vol 3, pp 2204–2207, https://doi.org/10.1109/IEMBS.2001.1017209

Nie R, He M, Cao J, Zhou D, Liang Z (2018) Pulse coupled neural network based mri image enhancement using classical visual receptive field for smarter mobile healthcare. J Ambient Intell Humaniz Comput. https://doi.org/10.1007/s12652-018-1098-3

Pirhonen M, Peltokangas M, Vehkaoja A (2018) Acquiring respiration rate from photoplethysmographic signal by recursive bayesian tracking of intrinsic modes in time-frequency spectra. Sensors (Basel) 18(6):1693. https://doi.org/10.3390/s18061693

Ps KB, Jatti A (2015) Respiration and heart rate monitoring from photoplethysmograph signal. Adv Sig Process 3(1):8–16. https://doi.org/10.13189/asp.2015.030102

Sanyal S, Nundy KK (2018) Algorithms for monitoring heart rate and respiratory rate from the video of a user's face. IEEE J Transl Eng Health Med 6:1–11. https://doi.org/10.1109/JTEHM.2018.2818687

Schroeder CA, Smith LJ (2011) Respiratory rates and arterial blood-gas tensions in healthy rabbits given buprenorphine, butorphanol, midazolam, or their combinations. Journal of the American Association for Laboratory Animal Science : JAALAS 50(2):205–211, http://www.ncbi.nlm.nih.gov/pmc/articles/PMC3061421/

Singh M (2014) Introduction to Biomedical Instrumentation, 2nd edn. PHI Learning

Soltani S (2002) On the use of the wavelet decomposition for time series prediction. Neurocomputing 48(1):267–277. https://doi.org/10.1016/S0925-2312(01)00648-8, http://www.sciencedirect.com/science/article/pii/S0925231201006488

Tabei F, Kumar R, Phan TN, McManus DD, Chong JW (2018) A novel personalized motion and noise artifact (mna) detection method for smartphone photoplethysmograph (ppg) signals. IEEE Access 6:60498–60512. https://doi.org/10.1109/ACCESS.2018.2875873

Tambe SB, Gajre SS (2018) Cluster-based real-time analysis of mobile healthcare application for prediction of physiological data. J Ambient Intell Humaniz Comput 9(2):429–445. https://doi.org/10.1007/s12652-017-0562-9

Ubeyli ED, Guler I (2005) Feature extraction from doppler ultrasound signals for automated diagnostic systems. Comput Biol Med 35(9):735–64. https://doi.org/10.1016/j.compbiomed.2004.06.006

Unser M, Aldroubi A (1996) A review of wavelets in biomedical applications. Proc IEEE 84(4):626–638. https://doi.org/10.1109/5.488704

Webster JG (1997) Design of pulse oximeters, 1st edn. Institute of Physics Publishing, http://www.crcnetbase.com/isbn/9780750304672